

Bio-Derived material for supporting the efficiency of Sodium-Ion Batteries

Samira Bagheri¹, Majid Monajjemi², Alireza Ziglari^{1,*}

¹ Department of Chemistry, College of science, Central Tehran Branch, Islamic Azad University, Tehran, Iran

² Department of Chemical Engineering, Central Tehran Branch, Islamic Azad University, Tehran, Iran

*corresponding author e-mail address: maj.monajjemi@iauctb.ac.ir

ABSTRACT

The biologically derived material is a cost-effective and environmentally benign alternative to the used metal ion batteries. All biological cells such as human cells and bacterial cells contain ionic systems, with ion transport activities which respond to stimuli sensed by the environmental systems. During these processes, its energy is supplied by adenosine triphosphates (ATP), which exist as complex ions as well. In this study, the riboflavin is simulated as cathode material for sodium-ion batteries. Additionally, we have exhibited the structure of riboflavin/h-BN nano-hybridization can be to improve the capacities and the electrical transports in C-BN sheets-based anodes for NIBs. Riboflavin/h-BN nano-hybridization could also be assembled into free-standing electrodes without any binder or current collector, which will lead to increased specific energy density for the overall battery design. This work exhibits a foundation for the use of the bio-derived system, high-performance sodium-ion batteries.

Keywords: Riboflavin; vitamin B₂; sodium-Ion Batteries; Bio-derived material.

1. INTRODUCTION

Riboflavin (vitamin B₂) is used as a dietary supplement to prevent and treat riboflavin deficiency and prevent migraines. It is required by the body for cellular respiration; from food sources include eggs, green vegetables, milk, and meat [1]. It was discovered in 1920, isolated in 1933, and first synthesized in 1935 [1]. Riboflavin functions as a coenzyme is required for a protein of enzymes for performing a normal physiological action. Quinone can be found in important bio metabolism processes in nature such as photosynthesis and respiration, serving as charge - mediating agents via redox reactions. The active structure is flavin mononucleotide (FMN) and flavin adenine dinucleotide (FAD) function as cofactors for variety reactions such as flavo-proteins of electron transport chain, the production of pyridoxic acid from vitamin B₆ through pyridoxine 5'-phosphate oxidase, The primary coenzyme form pyridoxal phosphate, Oxidation of pyruvate, Fattyacyl dehydrogenase convert vitamin A to retinoic acid via cytosolic retinal dehydrogenase, Synthesis of an active form of folate (5-methyltetrahydrofolate) from 5,10-methylenetetrahydrofolate via methylen- hydro-folate reeducates, convert tryptophan to vitamin B₃ and Reduction of the oxidized form glutathione to its reduced form (GSH) [2-4]. Various forms of these kind systems have been studied as electrodes for secondary lithium-organic batteries in 1972 [5]. Another works concerning quinone derivative has applied on the energy densities and increasing of the capacities and redox potential which the simplest derivative as the name 1,4-benzoquinone, can deliver a theoretical capacity of 500 mili-Ah/g. Quinone derivatives with 1-3 aromatic rings have been investigated. 2,3,5,6-tetrahydroxy-1,4-benzoquinone, which has a theoretical capacity greater than 270 miliAh/g, exhibits a practical capacity of 200 miliAh/g in a lithium cell, which is comparable with the capacities of conventional layered transition metal oxide electrodes [6,7]. Quinone is

composed of aromatic ring with -(C=O) - groups, accompanied by the rearrangement of double bonds. Because the redox center of quinones is a C=O bond, multiple charges can be stored in a relatively compact structure, resulting in a high charge capacity. Quinone-based cathode exhibit moderately high reduction potentials (>2.1 V versus Li/Li⁺), which is attributed to the formation of an additional stable aromatic system upon reduction [8]. With the discovery of highly reversible, low-voltage Li-intercalation carbonaceous materials, Sony realized the commercialization of xC₆/Li_{1-x}CoO₂ cells in 1991 [1]. Lithium ion batteries (LIBs) are representative energy storage devices based on electrochemical energy, widely used in small grid storage systems. The favorable electrochemical performance of LIBs regarding energy and power densities, as well as the progress in cell design and manufacturing, have made LIBs greatly successful for mobile electronics. However, concerns regarding the future availability of lithium resources are rising. Sodium ion batteries (NIBs) have been drawing increasing attention because Na is an earth abundant element and shares common properties with Li [2-4].

Sodium-ion batteries are a type of reusable battery that uses sodium-ions as its charge carriers and Na-ion batteries are very similar to Li-ion batteries in many ways. Na ion is 30% larger in diameter and 2 times heavier within a lower gravimetric capacity than Li-ion batteries approximately. In addition Na metal is more active than Li with a standard electrode potential is ~0.3V higher than Li. However; the Na⁺ ion has a larger radius than the Li⁺ ion, which makes many of the superior LIB electrode materials unsuitable for NIBs. In particular, graphite is a widely used anode material for the present commercial LIBs, while it has been reported to have a very low capacity of when used as an anode for NIBs [9-11].

2. EXPERIMENTAL SECTION

2.1. Cathode materials.

Three cathode materials, NaCoO₂, NaMn₂O₄, and NaFePO₄, have represented the majority of NIBs cathode research. In an extended approach, they can be classified as 1-Layered compounds NaMO₂ (M = Co, Ni, Mn), 2- Spinel compounds NaM₂O₄ (M = Mn, etc.) 3- Olivine compounds NaMPO₄ (M = Fe, Mn, Ni, Co, etc.).

In this work, the quinones as the biologically derived material has replaced and simulated instead of those above cathodes materials via Tobacco mosaic virus (TMV). When a Na-ion diffuses out of the cathode (ionic conduction) during the charge cycle the valence state of the transition metal ion changes (electronic conduction); the Fe²⁺ ion is oxidized to Fe³⁺. The reaction in cathode can be written as: [quinones⁻]_{Na_x - xe⁻ ⇌ Na_(x)[quinones⁻] + Na_(1-x)[quinones⁻]. Thus, it is important that electrical and ionic conductivities be optimized in cathode materials since either of these values can dictate the overall cell properties including capacity and cycle life. To date, only conductive coatings and particle size reduction techniques have resulted in higher conductivity for cathode materials. Diffusion of a Na-ion in a cathode particle is strongly dependent upon the interaction potential between the Na-ion and the host material structure. This model describes the diffusion path as the following: W_T = W_C + W_P + W_R (1). Where W_T is the total potential energy, W_C is the Columbic interaction, W_P is the van der Waals interaction and W_R is the overlap repulsion between closed shell ions.}

Synthesis using the virus can also be used for the fabrication of a nano-mixture cathode, enabling the construction of fully virus-built batteries [12]. The site of the coat protein of the virus, which attracts Fe³⁺ ions, acted as a growth site for amorphous FePO₄, and the end protein could bind to the riboflavin/hBN sheet. Using this multifunctional virus, it was possible to construct a nano-scale network structure between the FePO₄ and BN/sheet. The FePO₄- BN electrode displayed superior discharge capacity. The improved properties were attributed to the finely dispersed active materials (FePO₄), well-constructed electronic conducting path riboflavin/BN with simple reaction of NaFePO₄ - xNa⁺ - xe⁻ ⇌ x NaPO₄ + (1-x) NaPO₄ and Fe²⁺ - e⁻ ⇌ Fe³⁺ (2).

2.2. ANODE MATERIALS

In the case of the anode, Na metal is found to be the suitable electropositive with large reversible capacity. However, due to safety considerations, metallic Na has been substituted by various carbonaceous materials such as GO. GO-sodium anodes have much lower gravimetric and volumetric energy densities than pure sodium which lead towards the development of interstitial-free 3d transition metal oxides (M_xO_y, M = Fe, Co, Ni, Mn, Cu). These materials are able to incorporate more than one Na⁺ per metal through conversion reactions giving higher capacities in comparison to carbon anodes. Conduction in graphite and GO anodes are complex due to continuous phase transformations and the formation of the SEI layer. During discharge, Na⁺ ions are

extracted from the layered graphite, they pass through the electrolyte and intercalate between the cathode materials.

2.3. Electron density profile models.

The electron density has been defined as $\rho(r) = \eta_i |\varphi_i(r)|^2 = \sum_i \eta_i |\sum_l C_{li} \chi_l(r)|^2$ (3). [13] Where η_i is number of orbital (i), φ are orbital wave functions, χ are basis functions, the element of i_{th} row j_{th} column corresponds to the expansion coefficient of orbital j respect to basis functions i . Atomic units for electron densities can be explicitly written as e/Bohr³.

$$\nabla\rho(r) = \left[\left(\frac{\partial\rho(r)}{\partial(x)} \right)^2 + \left(\frac{\partial\rho(r)}{\partial(y)} \right)^2 + \left(\frac{\partial\rho(r)}{\partial(z)} \right)^2 \right]^{\frac{1}{2}} \quad (4) \quad \nabla^2\rho(r) = \frac{\partial^2\rho(r)}{\partial x^2} + \frac{\partial^2\rho(r)}{\partial y^2} + \frac{\partial^2\rho(r)}{\partial z^2} \quad (5) \quad [13].$$

The (+) and (-) values of these functions correspond to electron densities are locally depleted and locally concentrated respectively. The relationships between $\nabla^2\rho$ and valence electron shells (electron pair repulsion) (VSEPR) model, chemical bonds, electron localization and chemical reactivities have been built by the Bader work [14].

The kinetic energies densities are not individually defined, since the expected values of kinetic energies operators

$\langle \varphi | - \left(\frac{1}{2} \right) \nabla^2 | \varphi \rangle$ can be recovered by integrating kinetic energies densities from an alternative definition.. The general definition is: $k(r) = -\frac{1}{2} \sum_i \eta_i \varphi_i^*(r) \nabla^2 \varphi_i(r)$ (6) depends to $K(r)$, the local kinetic energies definition given below guarantee positives everywhere; hence the physical meaning is clearer and is more generally used. The Lagrangian kinetic energies densities, “G(r)” are also known as positive parameter of kinetic energies densities.

$$G(r) = \frac{1}{2} \sum_i \eta_i |\nabla(\varphi_i)|^2 = \frac{1}{2} \sum_i \eta_i \left\{ \left[\left(\frac{\partial\varphi_i(r)}{\partial(x)} \right)^2 + \left(\frac{\partial\varphi_i(r)}{\partial(y)} \right)^2 + \left(\frac{\partial\varphi_i(r)}{\partial(z)} \right)^2 \right] \right\} \quad (7).$$

$K(r)$ and $G(r)$ are directly related by Laplacian of electron density $\frac{1}{4} \nabla^2 \rho(r) = G(r) - K(r)$ (8)

2.4. Electron localization function (ELF)

Becke [15] and Edgecombe noted that spherically averaged like spin conditional pair probability has direct correlation with the Fermi hole and then suggested electron localization function (ELF) [124]. $ELF(r) = \frac{1}{1+[D(r)/D_0(r)]^2}$ (9)

$$\text{where } D(r) = \frac{1}{2} \sum_i \eta_i |\nabla\varphi_i|^2 - \frac{1}{8} \left[\frac{|\nabla\rho_\alpha|^2}{\rho_\alpha(r)} + \frac{|\nabla\rho_\beta|^2}{\rho_\beta(r)} \right] \quad (10) \quad \text{and}$$

$$D_0(r) = \frac{3}{10} (6\pi^2)^{\frac{2}{3}} [\rho_\alpha(r)^{\frac{5}{3}} + \rho_\beta(r)^{\frac{5}{3}}] \quad (11) \quad \text{for close-shell system,}$$

since $\rho_\alpha(r) = \rho_\beta(r) = \frac{1}{2} \rho$, D and D_0 terms can be simplified

$$\text{as } D(r) = \frac{1}{2} \sum_i \eta_i |\nabla\varphi_i|^2 - \frac{1}{8} \left[\frac{|\nabla\rho|^2}{\rho(r)} \right] \quad (12), \quad D_0(r) = \frac{3}{10} (3\pi^2)^{\frac{2}{3}} \rho(r)^{\frac{5}{3}}$$

(13). Savin [16] *et al* has reinterpreted ELF's in view point of kinetic energies, which makes ELF's meaningful for the Kohn-Sham DFT waves-function or post-HF wave-functions. They indicated that $D(r)$ reveals the excess kinetic energies densities caused by Pauli repulsions, while $D_0(r)$ can be considered as Thomas-Fermi kinetic energies densities. Localized orbital locator (LOLs) are another function for locating high localization region

likewise ELF, defined by Schmider and Becke[13]. $LOL(r) = \frac{\tau(r)}{1+\tau(r)}$ (14), where $(r) = \frac{D_0(r)}{\frac{1}{2}\sum_i \eta_i |\nabla\phi_i|^2}$ (15), $D_0(r)$ for spin-polarized systems and close-shell systems are defined in the same waies as the ELFs [13].

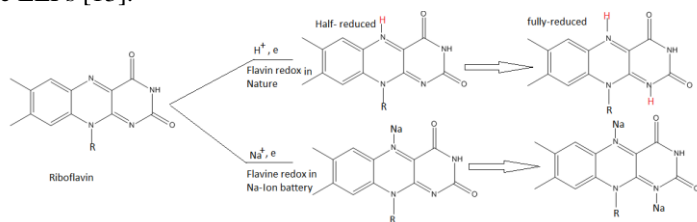


Fig. 1. Redox mechanism and chemical reaction of quinone based electrode materials.

Local information entropy is a quantification of information, this theory was proposed by Shannon in his study of information transmission in noise channel, and nowadays its application has been largely widened to other areas, including theoretical chemistry. For example, Aslangul and coworkers attempted to decompose diatomic and triatomic molecules into mutually exclusive space by minimizing information entropy [13]. We simulated our systems based on some previous works [17-32].

2.5. Computational details.

Calculations were accomplished using both Gaussian and GAMESS-US packages. In the present work, we have mainly focused for getting the optimized results of each tube from the DFT methods within the M06, M06-L and M06-HF post DFT methods. The m062x, m06-L, and m06-HF are novel Meta hybrids DFT functional with the good correspondences in a non-bonded calculation and are used for calculating the energies of the distances among the plates of h-BN sheets. Pm6, Extended-Huckel, and Pm3MM including pseudo=lanl2 calculations using the Gaussian program have done for the non-bonded interaction between two tubs. M06 and m06-L (DFT) functionalism are based on an iterative solution of the Kohn-Sham equations for the

density functional theories in the plane-waves set with the projector-augmented waves pseudo-potentials. The Perdew-Burke-Ernzerhof (PBE) exchange-correlations (XC) functional of the generalized gradient approximations (GGA) are adopted. The optimizations of the lattice constants and the atomic coordinates are made by the minimization of the total energies.

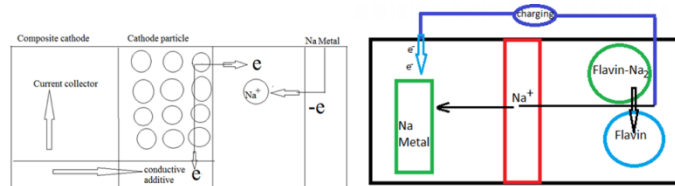


Fig. 2. The conduction phenomena in cathode particle (NaFePO_4) in charge

We employed densities functional theories with the van der Waals density functional for modeling the exchange-correlations energies of h-BN sheets. The double ζ -basis set with polarization orbitals (DZP) were used for riboflavin over the h-BN sheets.

For non-covalent interactions between riboflavin and h-BN sheet, the B3LYP calculations are unable for describing van der Waals capacitors systems by medium-ranges interactions) such as the interactions of two cylinders). The B3LYP method and most other functions are generally insufficient for illustrating the exchange and correlation energies in distant non-bonded medium-range systems. Moreover, some recent studies have been shown that inaccuracy for the medium-range exchange energies leads to large systematic errors in the prediction of molecular properties. We further calculated the interaction energy between riboflavin and h-BN sheets. The interaction energy was calculated via the Mp6 method in all items according to $\Delta E_S(eV) = \{E_{total} - (E_{hBN} + E_{riboflavin})\} + E_{BSSE}$ (16) Where the “ ΔE_S ” is the stability energy of system.

7. RESULT AND DISCUSSION

The data of densities, energies, electron localization functions (ELFs), Localized orbital locator (LOLs) and Local Entropies, Gap energies, charges from ESP, electrostatic potentials, Ionization energies, the Charges of Riboflavin/h-BN systems and the stability energies of h-BN sheets (tables1-2) and whole data have been listed and plotted in seven figures (figs.1-7) and 3 tables.

Table 1. Density, energy, Electron localization function (ELF), The localized orbital locator (LOL) and Local Entropy for sodium-riboflavin/h-BN system.

Sodium No.	Density of all electron $\times (10^{-3})$	Density of α electron $\times (10^{-4})$	Density of β electron $\times (10^{-4})$	Spin density of electron	Potential energy density $\times (10^{-3})$	LOL $\times 10^3$	Ellipticity $\times 10^{-7}$	ELF $\times 10^{-7}$	Eta index
Na(1)	0.22	0.11	0.11	0.0	-0.10	0.12	-0.32	0.14	0.11
Na(2)	0.26	0.13	0.13	0.0	-0.22	0.14	-0.26	0.17	0.10
Na(3)	0.20	0.1	0.1	0.0	-0.24	0.16	-0.22	0.15	0.12
Na(4)	0.24	0.12	0.12	0.0	-0.22	0.14	-0.23	0.14	0.11

We have calculated the gradient norms and the Laplacian of electrons densities via Eqs (3-5) for the sodium diffused in the riboflavin/h-BN sheets (Table2). For calculating the electrons spin densities from the difference between alpha and beta densities, we have used $\rho^s(r) = \rho^\alpha(r) - \rho^\beta(r)$ then the spins polarization

parameter functions will be returned instead of spin densities

$$\xi(r) = \frac{\rho^\alpha(r) - \rho^\beta(r)}{\rho^\alpha(r) + \rho^\beta(r)}$$

The absolute values of ξ going from zero to unity correspond to the local region going from un-polarized cases to completely polarized cases (Table1). The kinetic energies densities, Lagrangian kinetic energies densities, and the electrostatic potentials from nuclear / atomic charges can be calculated as eqs. (6-8).

Table 2. Charge from ESP, electrostatic potential and Ionization energy for each Na of 4 sodium diffused.

Sodium No.	Charge from ESP a.u.	Electrostatic Properties a.u.	Average Local Ionization Energy $\times 10^{-8}$	Hole For a
Na(1)	0.94	-0.14	0.60	-0.11
Na(2)	0.95	-0.11	0.70	-0.12
Na(3)	0.96	-0.12	0.75	-0.18
Na(4)	0.97	-0.12	0.80	-0.16

The larger electrons localizations are in the region, the more likely the electrons motion are confined within it. If the electrons are completely localized, then they might be distinguished from the ones outside. Bader finds that the regions which have larger electrons localization must have a larger magnitudes for Fermi holes integration. However, the Fermi holes are six-dimension functions and thus it is hard to be studied visually. Since $D_0(r)$ from eqs 9-12 is introduced into ELF's as a reference, what the ELF's reveals is actually a relative localization. ELF's are within the range of [0, 1]. A larger ELF values mean that electrons are greatly localized, indicating that there are covalent bonds.

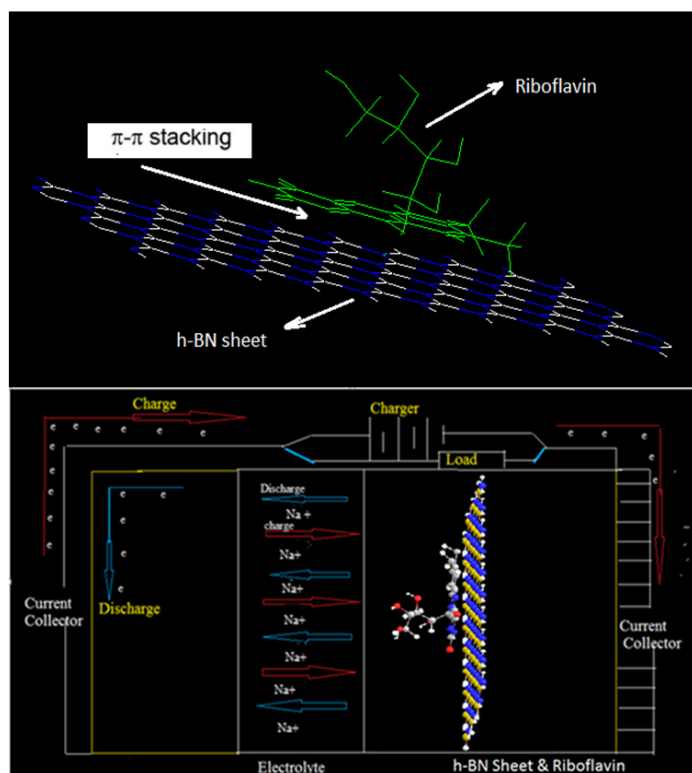


Fig. 3. Nano-hybridization of flavin molecules with h-BN through p-p stacking

ELF's have been widely used for the wide varieties of these systems, such as organic and inorganic small molecules, atomic crystals, coordination compounds, clusters, and also for some different problems, such as the revealing atomic shell structures, classification of chemical bonding, verification of charges-shifts bonds, studying Aromaticity. In which the actual kinetic energies terms in $D(r)$ from eqs. 12-14 are replaced by Kirzhnits types second-order gradient expansion, that is $\frac{1}{2} \sum_i \eta_i |\nabla \phi_i|^2 \approx D_0(r) + \frac{1}{72} \frac{|\nabla \rho|^2}{\rho(r) + \frac{1}{6} \nabla^2 \rho(r)}$ so that ELF's are totally independent from wave-functions, and then can be used for analyzing electron densities from X-ray diffraction data. Of course Tsirelson's ELF's can also be used for analyzing electron densities from quantum chemistry calculations, but are not as good as the ELF's defined by Becke owing to the approximation introduced in the kinetic energies term; however, qualitative conclusions can still be recovered basically.

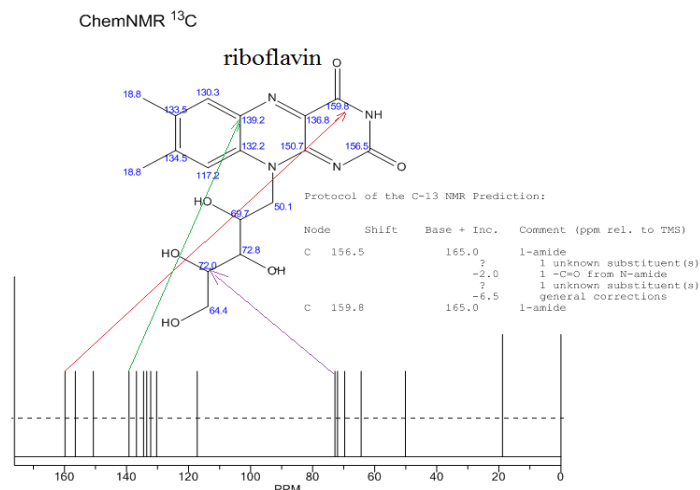


Fig. 4. Carbon NMR of riboflavin.

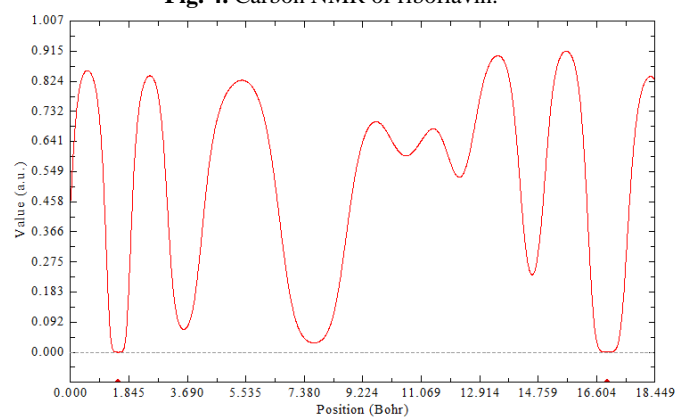


Fig. 5. ELF for riboflavin/h-BN system.

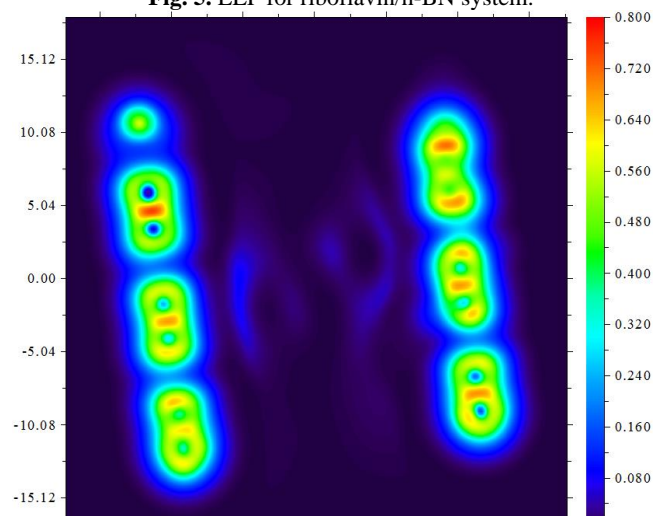


Fig. 6. Contour map of LOL for two electrodes

LOLs have similar expression such as to ELF's. Obviously, the chemical significant rats are generally qualitative and quantitative comparable, Since Jacobsen mentioned that LOL conveys much more deceives and clearer image than ELF, Actually, LOLs might be interpreted in the kinetic energies way as the ELF's; however, LOLs can also be interpreted in view point of localized orbitals. Small (large) LOLs value usually appear in boundary (inner) regions of localized orbitals because the gradient of orbitals wave-functions are large (small) in this area. The value range of LOLs is identical to ELF's, namely [0, 1]. In this work we have calculated the local Information entropy for each Sodium atom via eqs. 19-20 and the integrating of this function over whole spaces yield the information entropies.

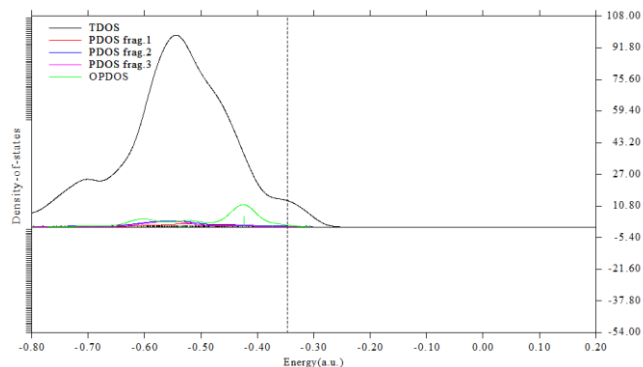


Fig. 7. Densities of states for cathode based riboflavin.

The data of local Information entropy are listed in Tables 1-3. Weak interaction (equation 16) have significant influences on the conformations of macromolecules; however reproductions of electrons densities by *AB-initio* calculations of reduced densities

8. CONCLUSION

In conclusion, we have performed our calculations to study the riboflavin adsorption on h-BN sheet with. Our results show that adsorption in is much stronger than the commercial battery.

Additionally, we have found the structure of riboflavin/h-BN might be increase the electrical transports in NIBs, So, the modification and designing of h-BN structures strategies for

9. REFERENCES

- [1] Squires V.R., The Role of Food, Agriculture, Forestry and Fisheries in Human Nutrition - Volume IV, *EOLSS publications*, 121, **2011**.
- [2] Mastropasqua L., Collagen cross-linking: when and how? A review of the state of the art of the technique and new perspectives, *Eye and vision*, (London, England), 2, 19, **2015**.
- [3] Yonemura S., Doane S., Keil S., Goodrich R., Pidcoke H., Cardoso M., Improving the safety of whole blood-derived transfusion products with a riboflavin-based pathogen reduction technology, *Blood transfusion Del segue.*, 15, 4, 357–364, **2017**.
- [4] Gropper S.S., Smith J.L., Groff J.L., Ch. 9: Riboflavin". *Advanced Nutrition and Human Metabolism*, 5th ed., Wadsworth: CENGAG Learning, 329–33, **2009**.
- [5] Alt H., Binder H., Köhling A., Sandstede G., Investigation into the use of quinone compounds-for battery cathodes, *Electrochim. Acta*, 17, 873–887, **1972**.
- [6] Chen H., Armand M., Courty M., Jiang M., Grey C.P., Dolhem F., Tarascon J.-M., Poizot P., Lithium salt of tetrahydroxybenzoquinone: toward the development of a sustainable Li-ion battery, *J. Am. Chem. Soc.*, 131, 8984–8988, **2009**.
- [7] Lei Z., Wei-kun W., An-bang W., Zhong-bao Y., Shi C., Yu-sheng Y., A MC/AQ parasitic composite as cathode material for lithium battery, *J. Electrochem. Soc.*, 158, A991–A996, **2011**.
- [8] Häupler B., Wild A., Schubert U.S., Carbonyls: powerful organic materials for secondary batteries, *Adv. Energy Mater.*, 5, 1402034, **2015**.
- [9] Yang Z.G., Zhang J.L., Kintner-Meyer M.C.W., Lu X.C., Choi D.W., Lemmon J.P., Liu J., *Chem. Rev.*, 111, 3577–3613, **2011**.
- [10] Schniepp H.C., Li J.L., McAllister M.J., Sai H., Herrera-Alonso M., Adamson D. H., Prud'Homme R. K., Car R., Saville D. A., Aksay I. A., Functionalized single graphene sheets derived from splitting graphite, *The Journal of Physical Chemistry*, B, 110, 17, 8535–8539, **2006**.
- [11] Lee Y.J., Yi H., Kim W.-J., Kang K., Yun D.S., Strano M.S., Ceder G., Belcher A.M., Fabricating genetically engineered high-power lithium-ion batteries using multiple virus genes, *Science*, 324, 1051–1055, **2009**.
- [12] Oh D., Qi J., Han B., Zhang G., Carney T.J., Ohmura J., Zhang Y., Shao-Horn Y., Belcher A.M., M13 virus-directed synthesis of nanostructured metal oxides for lithium–oxygen batteries, *Nano Lett.*, 14, 4837–4845, **2014**.

gradient (RDG) for such large systems are always take time-consuming. As sodium atoms have unpaired electrons, leading to a difference in spins-up and spins-down when two sodium atoms are adsorbed simultaneously electrons get paired and magnet moment disappears in the system. Consequently, spin polarized clusters have a gap which depends on adsorbed electrons spins polarization. In Table 3 a comparison between commercialized and bio-inspired redox-active electrode materials are listed.

Table 3. Theoretical Voltage and capacity for various systems

Material	Graphene-NaCoO ₂	Graphene-NaFePO ₄	h-BN-Riboflavin
Theoretical capacity	284	184	320
Voltage	3.8	3.4	2.6

improving the performance of riboflavin-based cathodes. During the increasing of density h-BN sheets, maximum capacities obtained are much higher than the commercial cathodes. This study will helps us to create better cathodes materials which can be replaced with a higher capacity and better cycling performance for NIBs.

- [13] Lu T., Chen F., Multiwfn: A Multifunctional Wavefunction Analyzer, *J. Comp. Chem.*, 33, 580-592, **2012**.
- [14] Bader R.F.W., Atoms in Molecule: A quantum Theory, *Oxford Univ. press*, Oxford, **1990**.
- [15] Becke, Edgecombe, A simple measure of electron localization in atomic and molecular systems, *The Journal of Chemical Physics*, 92, Issue 9, 1, 1990, 5397-5403, **1990**.
- [16] Savin et al., *Angew. Chem. Int.*, Ed.Engl., 31, 187, **1991**.
- [17] Monajjemi M., Mohammadian N.T., S - N I C S : An Aromaticity Criterion for Nano Molecules, *J. Comput. Theor. Nanosci.*, 12, 4895-491, **2015**.
- [18] Monajjemi M., Lee V.S., Khaleghian M., Honarparvar B., Mollaamin F., Theoretical Description of Electromagnetic Nonbonded Interactions of Radical, Cationic, and Anionic NH₂BHNH₂ Inside of the B₁₈N₁₈ Nanoring, *J. Phys. Chem. C.*, 114, 15315, **2010**.
- [19] Monajjemi M., Boggs J.E., A New Generation of BnNn Rings as a Supplement to Boron Nitride Tubes and Cages, *J. Phys. Chem. A*, 117, 1670–1684, **2013**.
- [20] Monajjemi M., Non bonded interaction between BnNn (stator) and BN B (rotor) systems: A quantum rotation in IR region, *Chemical Physics.*, 425, 29-45, **2013**.
- [21] Monajjemi M., Wayne Jr, R., Boggs J.E., NMR contour maps as a new parameter of carboxyl's OH groups in amino acids recognition: A reason of tRNA–amino acid conjugation, *Chemical Physics.*, 433, 1-11, **2014**.
- [22] Monajjemi M., Quantum investigation of non-bonded interaction between the B₁₅N₁₅ ring and BH₂NBH₂ (radical, cation, anion) systems: a nano molecularmotor, *Struct Chem*, 23, 551–580, **2012**.
- [23] Monajjemi M., Non-covalent attraction of B₂N (2,0) and repulsion of B₂N(+) in the BnNn ring: a quantum rotatory due to an external field, *Theor Chem Acc*, 134, 77,1-22, **2015**.
- [24] Monajjemi M., Metal-doped graphene layers composed with boron nitride–graphene as an insulator: a nano-capacitor, *Journal of Molecular Modeling*, 20, 2507, **2014**.
- [25] Monajjemi M., Cell membrane causes the lipid bilayers to behave as variable capacitors: A resonance with self-induction of helical proteins, *Biophysical Chemistry*, 207, 114–127, **2015**.

- [26]. Soofi N. S., Monajjemi, M, A Study of Fe₃O₄ @ Si₁₈O₂₇ Catalyst through Statistical-Nucleus Independent Chemical Shifts (S-NICS) Method, *Orient. J. Chem*, 32 , 5 , 2327-2345 , **2016**.
- [27]. Jalilian H., Monajjemi M ., Aghaei H., X-doped Graphene Interaction with Anodic Material LIBs, *Orient. J. Chem*, 33 , 5 , 2179-2187 , **2017**.
- [28]. Moosavi M. S., Monajjemi M.,; Zare K., A Nano Catalyst of CoFe₂O₄@ B₁₈N₁₈ as A Novel Material, *Orient. J. Chem*, 33 , 4 , 1648-1658, **2017**.
- [29] Chitsazan A., Monajjemi M., Aghaei H., Neutral Gases Adsorption With Hydrogen on Silicon Nanotubes: A Fuel Cell Investigation *Orient. J. Chem* , 33,3,1366-1374 , **2017**.
- [30] Monajjemi M., Liquid-phase exfoliation (LPE) of graphite towards graphene: An ab initio study, *Journal Of Molecular Liquids*, 230, 461-472 , **2017**.
- [31]. Zakeri M., Monajjemi M., Effective molecules of some natural product as antidepressant and antihistamine drugs: A NMR study, *Ukrainian Journal of Ecology* , 8 , 2, 255-262 , **2018**.
- [32] Fu K..K., et al. All-component transient lithium-ion batteries. *Adv. Energy Mater.* 6, 1502496 ,**2016**.

© 2018 by the authors. This article is an open access article distributed under the terms and conditions of the Creative Commons Attribution license (<http://creativecommons.org/licenses/by/4.0/>).